MOLECULAR PHYSICS
https://doi.org/10.1080/00268976.2018.1471234

Taylor & Francis
Taylor & Francis Group

FRENKEL SPECIAL ISSUE

A correlation-hole approach to the electric double layer with counter-ions only

Ivan Palaia[a], Martin Trulsson[b], Ladislav Šamaj[c] and Emmanuel Trizac[a]

[a]LPTMS, CNRS, Université Paris-Sud, Université Paris-Saclay, Orsay, France; [b]Theoretical Chemistry, Lund University, Lund, Sweden; [c]Institute of Physics, Slovak Academy of Sciences, Bratislava, Slovakia

ABSTRACT

We study a classical system of identically charged counter-ions near a planar wall carrying a uniform surface charge density. The equilibrium statistical mechanics of the system depends on a single dimensionless coupling parameter. A new self-consistent theory of the correlation-hole type is proposed which leads to a modified Poisson–Boltzmann integral equation for the density profile, convenient for analytical progress and straightforward to solve numerically. The exact density profiles are recovered in the limits of weak and strong couplings. In contrast to previous theoretical attempts of the test-charge family, the density profiles fulfil the contact-value theorem at all values of the coupling constant and exhibit the mean-field decay at asymptotically large distances from the wall, as expected. We furthermore show that the density corrections at large couplings exhibit the proper dependence on coupling parameter and distance to the charged wall. The numerical results for intermediate values of the coupling provide accurate density profiles which are in good agreement with those obtained by Monte Carlo simulations. The crossover to mean-field behaviour at large distance is studied in detail.

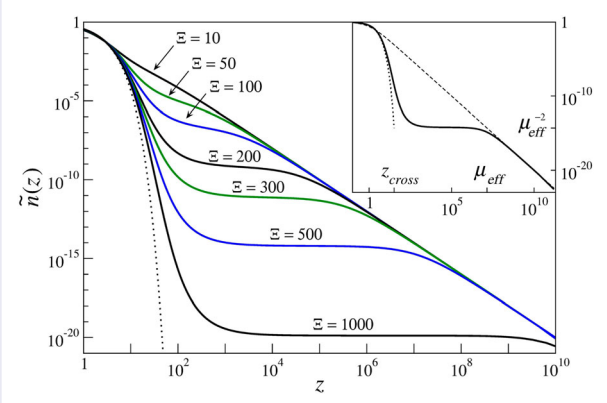

ARTICLE HISTORY
Received 1 March 2018
Accepted 15 April 2018

KEYWORDS
statistical mechanics; electric-double layer; correlation-hole; planar interfaces

1. Introduction

Experiments with large macromolecules are often performed in water, which is a polar solvent. This is the case for many applications using colloids, including the proteins in our bodies. This results in the release of low valence micro-ions into the solution, so that the colloids acquire a surface charge density, opposite to the charge of mobile micro-ions (coined as 'counter-ions'). The total surface charge can exceed thousands of elementary charges e. In the first approximation, the curved surface of a macromolecule can be replaced by an infinite planar wall.

The charged macromolecule and the surrounding counter-ions form a neutral electric double layer, see reviews [1–3]. In turn, the double layer is paramount in mediating the effective interactions between charged bodies in solution. At large enough Coulombic coupling, it is for instance known that like-charged macromolecules can effectively attract each other in some intermediate distance range, as was observed experimentally [4–9] and by computer simulations [10–13].

In a wealth of natural or synthetic systems, micro-ions can be of both signs, with positively and negatively charged species. In this paper, we restrict ourselves to

CONTACT Emmanuel Trizac trizac@lptms.u-psud.fr LPTMS, CNRS, Université Paris-Sud, Université Paris-Saclay, Orsay 91405, France

simplified so-called salt-free (or deionised) Coulomb systems with counter-ions only. This is a convenient starting point for analytical progress, where detailed computer simulation results are also available [14–28]. Such models apply to deionised suspensions, see e.g. the experiments reported in Refs. [29–33]. In the deionised limit, systems of counter-ions near charged surfaces have poor screening properties, but the standard Coulomb sum rules relating the one-body and two-body densities do apply [34,35].

For the system of counter-ions near a charged wall, the high-temperature (weak-coupling, WC) limit is described by the Poisson–Boltzmann (PB) mean-field theory [36] and by its systematic improvement via the loop expansion [16,37,38]. The opposite strong coupling (SC) limit was investigated within a field-theoretical formulation of the model by using a renormalised expansion of virial type [17,18,39–42]. In the leading SC order and in the present planar geometry, the counter-ions effectively behave as non-interacting objects, as far as one is not interested in the tail of the density profile; this fact was confirmed numerically in a number of numerical studies [43–48]. The first correction to the single-particle density profile, calculated within a fugacity expansion with a renormalisation of infrared divergences [18], is correct in its functional form, but with a wrong prefactor, departing by orders of magnitude from its Monte Carlo (MC) estimate [22]. Other SC approaches [49] emphasise the two-dimensional Wigner crystallisation of mobile charges at the wall surface for low temperatures. Recently [50], by a perturbative approach around the Wigner crystal, the single particle treatment was recovered in the leading SC order. Moreover, the derived prefactor of the first SC correction is in excellent agreement with MC simulations, also in the coupling range where no Wigner crystal is formed (strongly modulated liquid regime). Noteworthy are also field theoretic techniques, that allow to cover the crossover regime between WC and SC, by a proper splitting of the interactions between ions, discriminating short and long distances [21,22,25,51].

For a system of identical charges with Coulomb repulsion, the pair correlation function is strongly depleted at small distances. This gives credit to the image of a correlation hole around each ion in the system, an idea that turned useful in various approaches going beyond the PB theory [21,22,25,40,52–56]. Recently [28], for a dielectric interface, the single particle strong-coupling view was combined with the idea of the correlation hole, to obtain very accurate density profiles for strongly to moderately coupled charged fluids. This latter contribution provides the most accurate theory available so far for these systems. We emphasise that this approach is not self-consistent and does not reproduce mean-field PB results at small couplings, two key differences with the theory to be developed below.

In Ref. [20], an attempt has been made to establish a universal theory which works adequately for any value of the coupling. Based on a mean-field treatment of the ions response to the presence of a test charge, the exact density profile was reproduced in the limits of weak and strong couplings. For intermediate values of the coupling, the obtained approximate density profiles agree with MC simulations, except for two shortcomings. First, the contact theorem for the counter-ion number density at the wall [57–59] is not satisfied.Second, although a crossover from exponential to algebraic decay is observed at large distances from the wall, there is an additional prefactor to the mean-field PB solution which depends on the coupling constant. This is in contradiction with the common expectation that mean-field should hold at large distances from the wall [18,21,22,39,56,60], as the small density of counter-ions should effectively drive the system into the WC regime. Note that the loop corrections to the PB solution [16,37,38] are consistent with this expectation.

In this work, we propose a self-consistent theory for counter-ions near a charged planar wall, which is based on the idea of a cylindrical correlation hole. As was the case in the test-charge approach of Ref. [20], the exact density profiles are recovered in the limits of weak and strong couplings. But in contrast to that theory, at all values of the coupling constant do the density profiles fulfil the contact-value theorem. Moreover, the density profiles are exactly of mean-field type at asymptotically large distances from the wall, as expected. This allows us to address the elusive question of the asymptotic large distance crossover to mean-field in this geometry.

The article is organised as follows. In Section 2, we introduce the basic notations for the model. The correlation-hole approach is presented in Section 3. For the sake of analogy and completeness, the derivation of the PB theory is provided as well. Analytical progress was made possible by an original rederivation of the contact theorem that does not require the explicit resolution of the theory under study. Section 4 derives a number of exact results. The SC limit is worked out. Then, at arbitrary coupling parameter, the large-distance behaviour of the density profile is shown to be exactly of the PB mean-field type. In addition, we derive the subleading contribution to the mean-field tail. Numerical results for the density profile at specific values of the coupling constant are compared with those obtained by the test-charge method [20] and by MC simulations in Section 5. The crossover distance from the wall to the mean-field algebraic decay of the density profile is determined too. A short recapitulation and concluding remarks are given in Section 6, where we present some results pertaining to an

interacting two-plate system both in MC and within our self-consistent scheme.

2. Basic formalism

We consider the one-wall geometry pictured in Figure 1, with positions denoted by $\mathbf{r} = (x, y, z)$. A hard wall, impenetrable to particles, is localised in the half-space $\{\mathbf{r}, z < 0\}$. In the complementary half-space $\{\mathbf{r}, z > 0\}$, there are N mobile q-valent counter-ions (classical point-like particles) of charge $-qe$, where e is the elementary charge. The particles are immersed in a solution with the same dielectric constant ε as the confining wall, so that no electrostatic image forces ensue. The infinite wall surface, localised at $z = 0$, carries a fixed uniform surface-charge density σe with $\sigma > 0$. The system as a whole is electroneutral, and the particles are in thermal equilibrium at some inverse temperature $\beta = 1/(k_{\mathrm{B}}T)$.

There are two relevant length scales in the model. In Gauss units, two unit charges at distance r interact by the 3D Coulomb energy $\mathrm{e}^2/(\varepsilon r)$; the distance at which this energy coincides with the thermal energy $k_{\mathrm{B}}T$ is the Bjerrum length

$$\ell_{\mathrm{B}} = \frac{\beta \mathrm{e}^2}{\varepsilon}. \tag{1}$$

The potential energy of an isolated counter-ion of charge $-qe$ at distance z from the wall surface is given by

$$E(z) = \frac{2\pi q\, \mathrm{e}^2 \sigma}{\varepsilon} z; \tag{2}$$

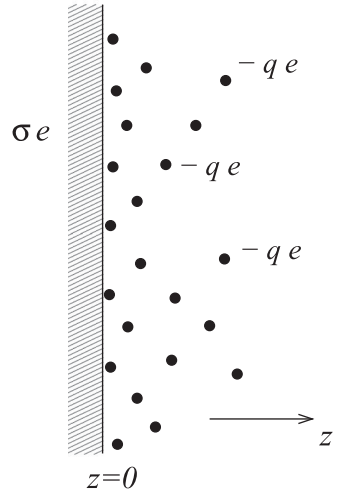

Figure 1. The electric double layer with counter-ions of valence q. The interface at $z = 0$ bears a surface charge σe, so that the system as a whole is electroneutral.

the distance at which this energy equals to the thermal energy $k_{\mathrm{B}}T$ defines the Gouy–Chapman length

$$\mu = \frac{1}{2\pi q \ell_{\mathrm{B}} \sigma}. \tag{3}$$

The dimensionless coupling parameter Ξ, reflecting the strength of electrostatic correlations, is defined as the ratio of the two length scales:

$$\Xi = \frac{q^2 \ell_{\mathrm{B}}}{\mu} = 2\pi q^3 \ell_{\mathrm{B}}^2 \sigma. \tag{4}$$

Denoting by $\langle \cdots \rangle$ the canonical thermal average, the particle number density at point $\mathbf{r}$ (with thus $z \geq 0$) is defined as $n(\mathbf{r}) = \langle \sum_{i=1}^{N} \delta(\mathbf{r} - \mathbf{r}_i) \rangle$. It depends only on the distance z from the wall, $n(\mathbf{r}) = n(z)$. The electroneutrality condition corresponds to the constraint

$$q \int_0^\infty \mathrm{d}z n(z) = \sigma. \tag{5}$$

The contact density of counter-ions at the wall is related to the surface charge density via the planar contact-value theorem [57–59] as follows:

$$n(0) = 2\pi \ell_{\mathrm{B}} \sigma^2. \tag{6}$$

The averaged particle density will be often written in a rescaled form with a dimensionless particle z-coordinate considered in units of the Gouy–Chapman length μ:

$$\tilde{n}(z) \equiv \frac{n(\mu z)}{2\pi \ell_{\mathrm{B}} \sigma^2}. \tag{7}$$

In terms of $\tilde{n}$, the electroneutrality requirement (5) and the contact-value constraint (6) take the forms

$$\int_0^\infty \mathrm{d}z \tilde{n}(z) = 1 \tag{8}$$

and

$$\tilde{n}(0) = 1, \tag{9}$$

respectively. To avoid unnecessarily heavy notations, z will in the remainder refer to the rescaled distance z/μ, whenever it appears in an expression involving the reduced density $\tilde{n}$.

The model is exactly solvable in two limits. In the weak-coupling limit $\Xi \to 0$, the PB approach [36] implies a slowly decaying particle density profile

$$\tilde{n}_{\mathrm{PB}}(z) = \frac{1}{(1+z)^2}. \tag{10}$$

In the strong-coupling limit $\Xi \to \infty$, the single-particle picture of counter-ions in the linear surface charge potential [17,18,56] leads to an exponentially decaying profile

$$\tilde{n}_{\mathrm{SC}}(z) = \exp(-z). \tag{11}$$

3. The correlation-hole approach

At any point $\mathbf{r}$ with $z \geq 0$, the relation between the (averaged) electric potential ψ and the charge distribution ρ is given by the Poisson equation. For the present geometry, the electrostatic potential and the charge distribution $\rho = -qen$ depend only on the distance from the wall z, so that

$$\frac{\mathrm{d}^2}{\mathrm{d}z^2}\psi(z) = \frac{4\pi}{\varepsilon}qen(z). \tag{12}$$

From the boundary condition at $z=0$, $\mathrm{d}\psi(z)/\mathrm{d}z = -4\pi\sigma e/\varepsilon$ and the 1D relation $\mathrm{d}^2|z|/\mathrm{d}z^2 = 2\delta(z)$ with δ the Dirac delta distribution, the electric potential is expressible explicitly as

$$\psi(z) = -\frac{2\pi}{\varepsilon}\sigma ez + \frac{2\pi}{\varepsilon}qe\int_0^\infty \mathrm{d}z'(|z-z'|-z')n(z'). \tag{13}$$

The interpretation of this expression is transparent: in addition to the bare plate potential (first term on the rhs, linear in z), the mobile counter-ions contribute to the electric potential though the integral term. The potential is determined up to an irrelevant constant; here we fixed the 'gauge' $\psi(0) = 0$.

3.1. PB theory

In the PB approach, the dimensionless density is written as

$$\tilde{n}_{\mathrm{PB}}(z) = \tilde{n}_0 \exp[\phi_{\mathrm{PB}}(z)], \tag{14}$$

where the PB reduced potential $\phi_{\mathrm{PB}} = \beta qe\psi_{\mathrm{PB}}$ is given by

$$\phi_{\mathrm{PB}}(z) = -z + \int_0^\infty \mathrm{d}z'(|z-z'|-z')\tilde{n}_{\mathrm{PB}}(z'). \tag{15}$$

Note the gauge $\phi_{\mathrm{PB}}(0) = 0$.

The normalisation constant $\tilde{n}_0$ is determined by the electroneutrality condition (8) through $1/\tilde{n}_0 = \int_0^\infty \mathrm{d}z \exp[\phi_{\mathrm{PB}}(z)]$. There exists a simple way to obtain the explicit value of $\tilde{n}_0$; it will prove useful below and we thus present it in its simplest clothing. We first differentiate the ϕ_{PB}-potential (15) with respect to z:

$$\frac{\mathrm{d}}{\mathrm{d}z}\phi_{\mathrm{PB}}(z) = -1 + \int_0^\infty \mathrm{d}z'\tilde{n}_{\mathrm{PB}}(z')\mathrm{sgn}(z-z'), \tag{16}$$

where sgn denotes the standard signum (sign) function. The integral

$$\int_0^\infty \mathrm{d}z\left(\frac{\mathrm{d}\phi_{\mathrm{PB}}}{\mathrm{d}z}+1\right)\tilde{n}_{\mathrm{PB}}(z) = \int_0^\infty \mathrm{d}z\int_0^\infty \mathrm{d}z'\tilde{n}_{\mathrm{PB}}(z)\tilde{n}_{\mathrm{PB}}(z')\,\mathrm{sgn}(z-z') \tag{17}$$

vanishes due to the anti-symmetric property of the function under integration in the rhs with respect to the interchange transformation $z \leftrightarrow z'$. From (14), we get

$$\tilde{n}_{\mathrm{PB}}(z)\frac{\mathrm{d}\phi_{\mathrm{PB}}}{\mathrm{d}z} = \frac{\mathrm{d}\tilde{n}_{\mathrm{PB}}(z)}{\mathrm{d}z}. \tag{18}$$

Consequently, we have from (17) that

$$\int_0^\infty \mathrm{d}z\frac{\mathrm{d}}{\mathrm{d}z}\tilde{n}_{\mathrm{PB}}(z) = -\int_0^\infty \mathrm{d}z\tilde{n}_{\mathrm{PB}}(z). \tag{19}$$

The density $\tilde{n}(z)$ vanishes as $z \to \infty$, so that

$$\tilde{n}_{\mathrm{PB}}(0) = \int_0^\infty \mathrm{d}z\tilde{n}_{\mathrm{PB}}(z) = 1, \tag{20}$$

which is nothing but the contact-value theorem (9). We see that, within the PB theory, the normalisation (8) automatically ensures the contact-value theorem (9), and vice versa. Under the gauge $\phi_{\mathrm{PB}}(0) = 0$, the contact-value relation (20) fixes $\tilde{n}_0 = 1$ in (14). It is easy to check that under this normalisation, the PB solution (10) satisfies Equations (14) and (15).

3.2. Inclusion of the correlation hole

In the single-particle SC solution (11), the only acting potential is due to the fixed surface-charge density; this potential is present also in the PB solution (14), but there is an additional potential related to the mean particle density profile. Thus in some sense, the SC solution is simpler than its mean-field counterpart, since mutual counter-ion interactions do not contribute to the leading order SC response. Yet, for large Ξ, counter-ions are strongly correlated in the (x, y) plane, because of their strong mutual repulsion; this leads to a marked correlation hole ('Coulomb hole'), inaccessible to other charged particles [18]. At smaller Ξ value, the correlation hole is less marked (in the sense that the pair correlation function does not vanish for distances smaller than the hole size [18]), but a feature of depletion remains. In addition, the form of the correlation hole depends on the distance from the wall of the particle under consideration. It is expected, in the large Ξ regime, that the correlation hole is cylindrical if the particle is close to the wall, and spherical for large distances from the wall (the bulk region) [20]. In this work, independently of the particle position with respect to the wall, we take as the correlation hole an infinite cylinder, perpendicular to the wall surface, whose axis passes through this particle. This picture is qualitatively related to that of a Wigner lattice of counter-ions near the charged wall that would prevail at very large coupling. Under smaller coupling parameters where no crystal is formed, a strongly modulated

liquid may remain that retains an essentially two dimensional feature. It shares with the crystal a well-defined correlation hole around each ion, the size of which stems from electroneutrality. The radius R of the cylinder is thus determined by the requirement that the total disc surface of all cylinders $\pi R^2 N$ equals the planar interface surface, namely

$$R^2 = \frac{q}{\pi\sigma} = 2q^2\ell_B\mu. \tag{21}$$

Note that, in units of the relevant Gouy–Chapman length μ, $R^2/\mu^2 = 2\Xi$, and up to an irrelevant prefactor, similar choices were made in [20,22]. This means that in units of μ, the correlation-hole radius R vanishes in the PB limit, while it goes to ∞ in the SC regime. Here, it can be stressed that μ is the relevant length scale for density gradients, both in the WC and SC regimes, as revealed by Equations (10) and (11).

The exclusion of other particles from the cylindrical neighbourhood of the given particle localised at z modifies the electric potential $\psi(z)$ (13) to $\psi_{ch}(z) = \psi(z) - \delta\psi(z)$, where

$$\begin{aligned}\delta\psi(z) &= \frac{1}{\varepsilon}\int_0^\infty dz' \int_0^R d\rho 2\pi\rho \frac{-qen(z')}{\sqrt{(z-z')^2+\rho^2}} \\ &= \frac{2\pi qe}{\varepsilon}\int_0^\infty dz' n(z') \\ &\quad \times [|z-z'| - \sqrt{R^2+(z-z')^2}].\end{aligned} \tag{22}$$

We take $\psi_{ch}(z)$ as the mean-field potential which determines the counter-ion density via $n(z) = n_0 e^{\beta qe\psi_{ch}(z)}$. We shift the reduced correlation-hole potential $\phi(z) = \beta qe\psi_{ch}(z)$ by a constant to fix the gauge $\phi(0) = 0$. Thus the rescaled density profile $\tilde{n}$ is given by

$$\tilde{n}(z) = \tilde{n}_0 \exp[\phi(z)], \tag{23}$$

where the reduced potential

$$\begin{aligned}\phi(z) &= -z + \int_0^\infty dz' \tilde{n}(z') \\ &\quad \times (\sqrt{2\Xi+(z-z')^2} - \sqrt{2\Xi+z'^2})\end{aligned} \tag{24}$$

satisfies the gauge $\phi(0) = 0$ and the normalisation constant $\tilde{n}_0$ is determined by the electroneutrality condition (8).

The explicit value of $\tilde{n}_0$ can be derived in close analogy with the above PB treatment. We first differentiate the ϕ-potential with respect to z:

$$\frac{d}{dz}\phi(z) = -1 + \int_0^\infty dz' \tilde{n}(z') \frac{z-z'}{\sqrt{2\Xi+(z-z')^2}}. \tag{25}$$

The integral

$$\begin{aligned}\int_0^\infty dz \left(\frac{d\phi}{dz}+1\right)\tilde{n}(z) &= \int_0^\infty dz \int_0^\infty dz' \tilde{n}(z)\tilde{n}(z') \\ &\quad \times \frac{z-z'}{\sqrt{2\Xi+(z-z')^2}}\end{aligned} \tag{26}$$

vanishes due to the anti-symmetric property with respect to the interchange $z \leftrightarrow z'$ of the function under integration in the rhs. Then the equality

$$\int_0^\infty dz \frac{d\tilde{n}}{dz} = -\int_0^\infty dz \tilde{n}(z) \tag{27}$$

implies the contact-value theorem

$$\tilde{n}(0) = \int_0^\infty dz \tilde{n}(z) = 1. \tag{28}$$

We see that, as is the case within PB theory, the density normalisation automatically ensures the validity of the contact-value theorem. This is a nontrivial and exact property of our Coulombic system [61] that an approximate or phenomenological theory may violate (in this respect, it is thus remarkable that PB theory does fulfil this condition). None of the theories presented in [20] or [22] do obey the contact theorem. The gauge $\phi(0) = 0$ fixes the normalisation constant $\tilde{n}_0 = 1$. The density profile then takes the form

$$\tilde{n}(z) = \exp[\phi(z)], \tag{29}$$

where the reduced potential $\phi(z)$ is given by (24).

To summarise at this point, our key relation is (29), supplemented by the closure relation (24). The latter expresses the test-particle potential ϕ in terms of the mean counter-ion density, in a self-consistent fashion.

4. Analytical results

To begin with, it is straightforward to realise that in the weak-coupling limit $\Xi \to 0$, the reduced potential (24) takes the PB form (15). Due to the same normalisation $\tilde{n}_0 = 1$, our correlation-hole profile (23) reduces to the PB one (14). In this section, we prove that our correlation-hole theory also provides the exact density profiles in the strong coupling limit, where a series expansion is constructed to account for corrections to SC. Then, we focus on the tail of the ionic profile, showing that it is of mean-field type, and working out at arbitrary Ξ the corresponding large-z correction to the dominant tail. All these results will be compared to numerical data in Section 5.

4.1. SC limit

In the SC limit $\Xi \to \infty$, assuming that $\tilde{n}$ is short-ranged (e.g. decaying exponentially) and all its moments exist, we can perform in Equation (24) the expansion

$$\sqrt{2\Xi + (z-z')^2} - \sqrt{2\Xi + z'^2} \sim \frac{(z-z')^2}{2\sqrt{2\Xi}} - \frac{z'^2}{2\sqrt{2\Xi}} \tag{30}$$

to obtain $\phi(z) = \phi_{\rm SC}(z) = -z$. Inserting this one-body potential due to the surface-charge density into (29) reproduces the SC solution (11).

To construct an expansion around the SC limit, we anticipate the systematic $1/\sqrt{\Xi}$-expansion of the density profile of the form

$$\tilde{n}(z) = \mathrm{e}^{-z}\left[1 + \sum_{k=1}^{\infty} \frac{f_k(z)}{(2\Xi)^{k/2}}\right] \tag{31}$$

with as-yet unknown functions $f_k(z)$. The contact theorem (9) fixes the values of these functions at the wall,

$$f_k(0) = 0, \tag{32}$$

and the normalisation (8) fixes their integrals over z,

$$\int_0^{\infty} \mathrm{d}z f_k(z) = 0. \tag{33}$$

Since $\phi(z) = \ln \tilde{n}(z)$, we have

$$\phi(z) = -z + \ln\left[1 + \sum_{k=1}^{\infty} \frac{f_k(z)}{(2\Xi)^{k/2}}\right]. \tag{34}$$

Consequently,

$$\frac{\mathrm{d}}{\mathrm{d}z}\phi(z) = -1 + \frac{1}{1 + \sum_{k=1}^{\infty} \frac{f_k(z)}{(2\Xi)^{k/2}}} \sum_{l=1}^{\infty} \frac{f_l'(z)}{(2\Xi)^{l/2}}. \tag{35}$$

At the same time, from (25) we get

$$\frac{\mathrm{d}}{\mathrm{d}z}\phi(z) = -1 + \int_0^{\infty} \mathrm{d}z' \mathrm{e}^{-z'}\left[1 + \sum_{k=1}^{\infty} \frac{f_k(z')}{(2\Xi)^{k/2}}\right] \times \frac{(z-z')}{\sqrt{2\Xi}}\left[1 + \sum_{l=1}^{\infty} \binom{-1/2}{l} \frac{(z-z')^{2l}}{(2\Xi)^l}\right]. \tag{36}$$

Comparing the last two relations, we obtain an infinite iterative sequence of equations which relate $f_l'(z)$ to all $f_k(z)$ with $k \le l-1$. It turns out that $f_k(z)$ is a polynomial of order $2k$, the absolute term is equal trivially to zero because of the contact condition (32).

The first correction to the SC profile reads as

$$f_1(z) = \frac{z^2}{2} - z. \tag{37}$$

Writing formally the SC density profile plus the first correction as

$$\tilde{n}(z) = \mathrm{e}^{-z}\left[1 + \frac{1}{\theta}\left(\frac{z^2}{2} - z\right)\right], \tag{38}$$

we have $\theta = \sqrt{2\Xi} = 1.414\sqrt{\Xi}$. This has to be compared with the very accurate estimate based on the Wigner crystal $\theta = 1.771\sqrt{\Xi}$ [50]. A similar result $\theta \propto \sqrt{\Xi}$ was obtained in Ref. [25]. On the other hand, the finding $\theta = \Xi$ of the renormalised virial expansion [18] fails in the dependence on Ξ. Indeed, MC simulations fully corroborate the $\theta \propto \Xi^{1/2}$ scaling [50].

The next expansion functions read

$$\begin{aligned} f_2(z) &= \frac{z^4}{8} - \frac{z^3}{2} + \frac{z^2}{2} - z, \\ f_3(z) &= \frac{z^6}{48} - \frac{z^5}{8} + \frac{z^4}{8} - \frac{z^3}{6} - \frac{z^2}{2} - z, \\ f_4(z) &= \frac{z^8}{384} - \frac{z^7}{48} + \frac{z^5}{6} - \frac{17z^4}{24} + z^3 - 3z^2 - 3z, \end{aligned} \tag{39}$$

etc. It is interesting that the normalisation constraint (33) is automatically ensured by respecting the contact relation (32), which can serve as a check of algebra. Note that, at arbitrary order of the expansion around the SC limit, the density profile is decaying exponentially.

4.2. Large-distance decay: asymptotic validity of PB

For any finite value of the coupling Ξ and at asymptotically large distances from the wall ($z \to \infty$), the exact density profile is expected to exhibit the PB power law behaviour (10) [18,21,22,39,56,60], $\tilde{n}(z) \sim 1/z^2$. It is worthwhile emphasising that this power law behaviour implies that the (unscaled) counter-ion density becomes independent of the surface charge density σ, thereby revealing a universal behaviour. An important feature of our theory is that this asymptotic behaviour indeed takes place, at variance with the approach of Ref. [20].

To prove this fact, let us first assume that at large distances

$$\tilde{n}(z) \underset{z\to\infty}{\sim} \frac{a}{z^2} \tag{40}$$

with some positive number a which might depend on Ξ. Since the positive density $\tilde{n}$ does not exhibit divergent singularities, it must be bounded from above at any point

z by the function

$$\tilde{n}(z) \leq \frac{A}{(1+z)^2}, \tag{41}$$

where $A \geq a$. For $\Xi = 0$ we can take $A = 1$, while in the SC limit $\Xi \to \infty$ we have $A = 4/e = 1.47152\ldots$. The precise value of A is immaterial, as long as it is finite. Writing -1 in Equation (25) as $-\int_0^\infty \mathrm{d}z'\tilde{n}(z')$, the potential derivative is expressed after simple algebraic manipulations as follows:

$$\frac{\mathrm{d}}{\mathrm{d}z}\phi(z) = -2\int_z^\infty \mathrm{d}z'\tilde{n}(z') - I_1(z,\Xi) + I_2(z,\Xi), \tag{42}$$

where

$$I_1(z,\Xi) = \int_0^z \mathrm{d}z'\tilde{n}(z')\left[1 - \frac{z-z'}{\sqrt{2\Xi + (z-z')^2}}\right],$$
$$I_2(z,\Xi) = \int_z^\infty \mathrm{d}z'\tilde{n}(z')\left[1 - \frac{z'-z}{\sqrt{2\Xi + (z-z')^2}}\right]. \tag{43}$$

Both $\tilde{n}(z')$ and the functions in square brackets are positive. Using the inequality (41), in the large-z limit the integrals are bounded from above by

$$I_1(z,\Xi) \leq A\frac{\Xi + \sqrt{2\Xi}}{z^2} + O\left(\frac{1}{z^3}\right),$$
$$I_2(z,\Xi) \leq A\frac{\sqrt{2\Xi}}{z^2} + O\left(\frac{1}{z^3}\right). \tag{44}$$

Considering these bounds in (42), it holds that

$$\frac{\mathrm{d}}{\mathrm{d}z}\phi(z) = -2\int_z^\infty \mathrm{d}z'\tilde{n}(z') + O\left(\frac{1}{z^2}\right). \tag{45}$$

Since $\phi(z) = \ln\tilde{n}(z)$, the asymptotic formula (40) implies that $\phi'(z) \sim_{z\to\infty} -2/z$. Inserting this asymptotic relation together with (40) into Equation (45), one gets $a = 1$. Consequently, at any finite value of the coupling Ξ, the asymptotic large-distance behaviour of the density profile is exactly of PB type, as was expected. This property is confirmed also by a numerical treatment of our correlation-hole equations in the following section.

4.3. Subleading asymptotic correction

It is possible to go one step further and to compute the large-z correction to the mean-field asymptotics (large-z analysis at fixed Ξ). We use the electroneutrality condition (8) to rewrite the correlation-hole relation (25) as follows:

$$\frac{\mathrm{d}}{\mathrm{d}z}\phi(z) = -2\int_z^\infty \mathrm{d}z'\tilde{n}(z') + I(z,\Xi), \tag{46}$$

where

$$I(z,\Xi) = \int_0^\infty \mathrm{d}z'\tilde{n}(z')\left[\frac{z-z'}{\sqrt{2\Xi + (z-z')^2}} - \frac{z-z'}{|z-z'|}\right]. \tag{47}$$

To proceed, we change variables $z \to u = (1+z)^{-1}$ and perform a small u expansion in Equations (46) and (47). Using the fact that $I(u,\Xi) = -\Xi u^2 + o(u^2)$, writing $n(u) = u^2 + \Delta n(u,\Xi)$ and keeping in mind that Δn is $o(u^2)$ but not necessarily $O(u^3)$, we get

$$-\frac{\partial^2\Delta n}{\partial u^2} + \frac{2}{u}\frac{\partial\Delta n}{\partial u} + 2\Xi u + o(u) = 0, \tag{48}$$

from which the correction to the PB asymptotics follows:

$$\tilde{n}(z) \sim \frac{1}{(1+z)^2} - \frac{2}{3}\Xi\frac{\log(1+z)}{(1+z)^3}. \tag{49}$$

As the exact loop-derived correction, it is of order Ξ and decays at large z like $z^{-3}\log(z)$ [16,37,38]. Yet, our $-2/3$ prefactor for the correction in Equation (49) is not equal to that reported in [16], which is -1. We mention here that repeating the analysis of [16] leads us to a corrected prefactor $-1/2$, closer to the present $-2/3$.

We shall see below that the predicted correction is indeed found in the numerical treatment of our self-consistent scheme. For large Ξ, however, it becomes practically impossible to reach the relevant distance range, and another contribution preempts that in Equation (49) for the range of available distances. This is discussed further below.

5. Numerical results

5.1. The methods

The correlation-hole integral equation for the rescaled density profile $\tilde{n}$, given in Equations (24) and (29), bears some similarities with the non-linear PB formulation. Solving it numerically is straightforward. In practice, an efficient numerical scheme was found to be the following. Rescaled distances z are first mapped onto a variable $x = (1+z)^{-1/2}$, such that $x \in [0,1]$. The resulting equations for $\phi(x)$ are then discretised on a regular grid with N points (N up to 2×10^5). We initialise the density to be of PB form, meaning that $\tilde{n}(x) = x^4$ (which results in an improved convergence), before an iterative resolution. Convergence is typically achieved in 100 iterations if fine properties are sought. It is important here to emphasise

that from a computational point of view, the resolution of our self-consistent equation is significantly faster and more convenient than the test charge approach [20], or the theory of Santangelo [22].

In parallel, we have performed a number of MC simulations in a quasi-2D geometry. Ewald summation techniques corrected for quasi-2D-dimensionality allow to account for long-range electrostatic interactions (see the Appendix, together with e.g. [62–64]). The MC results provide the correct reference behaviour of our system of point ions in the vicinity of a charged plate.

5.2. Comparison to MC results

The numerical results for the deviations from PB profiles, $\tilde{n} - \tilde{n}_{\rm PB}$, are presented for the coupling constants $\Xi = 1$, $\Xi = 10$ and $\Xi = 100$ in Figures 2–4, respectively. Our MC simulations are compared to the test-charge theory [20], to the hybrid field theory of Ref. [22] where long and short distances are treated separately and to the present correlation-hole approach. We see that for the small value $\Xi = 1$, the accuracy of the test-charge and correlation-hole theories is comparable. The hybrid field theory of Ref. [22] (which is solved at the expense of enhanced technical complexity) fares better at short distances, but worse for $z > 2$. For intermediate $\Xi = 10$, the accuracy of our approach is better. For relatively large $\Xi = 100$, our solid curve practically passes through MC data. The accuracy of our results improves upon increasing Ξ.

For the tail of the ionic profile, at larger distances than those in the previous graphs, we see in Figure 5 that the correlation-hole picture captures qualitatively

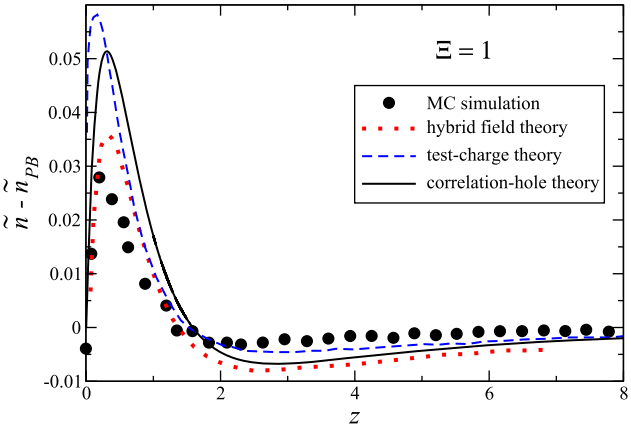

Figure 2. Deviation from the PB density profile, $\tilde{n} - \tilde{n}_{\rm PB}$, as a function of the dimensionless distance z for the coupling constant $\Xi = 1$. Symbols correspond to the results of MC simulation, the dashed curve is for the test-charge theory of Ref. [20], the dotted curve is for the approach of Ref. [22], and solid curve shows the present correlation-hole approach.

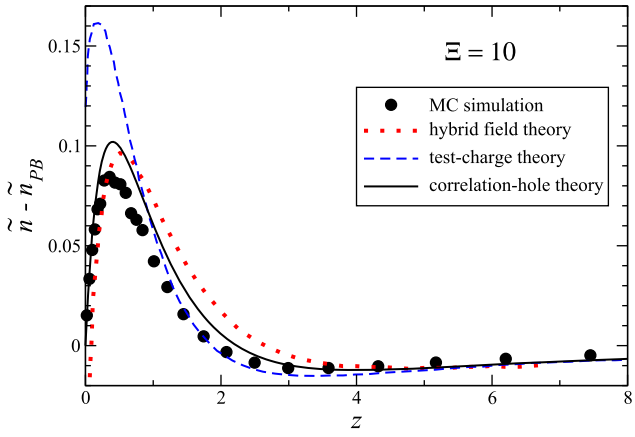

Figure 3. Same as Figure 2 for the coupling $\Xi = 10$.

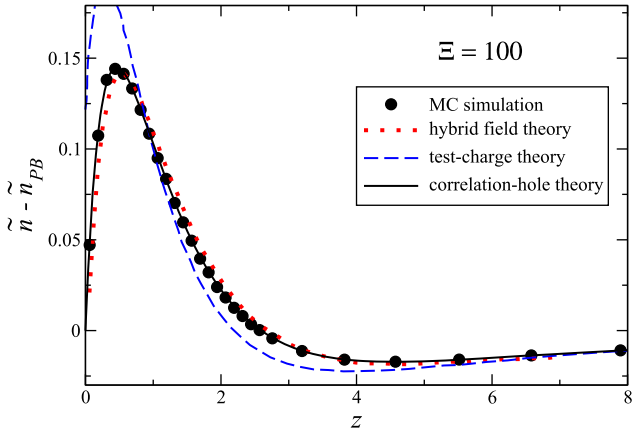

Figure 4. Same as Figure 2 for $\Xi = 100$.

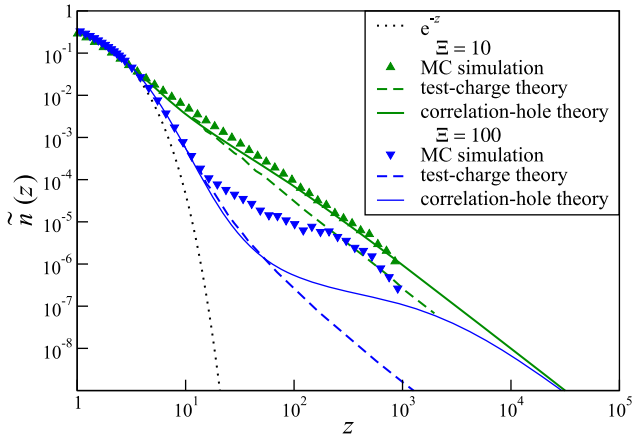

Figure 5. Large-distance counter-ion densities for $\Xi = 10$ and $\Xi = 100$. MC data (symbols) are compared to the correlation-hole results (solid curves) and those of the test-charge theory of Ref. [20] (dashed lines). The dotted line is for the SC limiting behaviour $\Xi \to \infty$.

the departure from SC behaviour, although in a distance range that is not close enough to the charged plate. Yet, the test charge theory fails in getting the qualitative

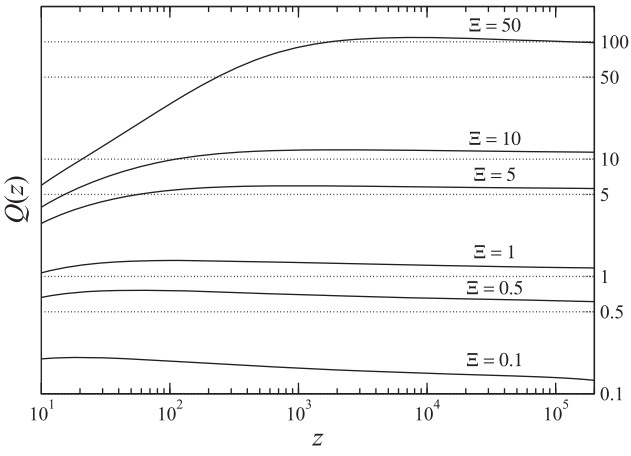

Figure 6. Plot of $Q(z)$ as defined in Equation (50) vs distance to the charged wall. Equation (49) predicts that Q asymptotically tends to Ξ, indicated by horizontal dotted lines.

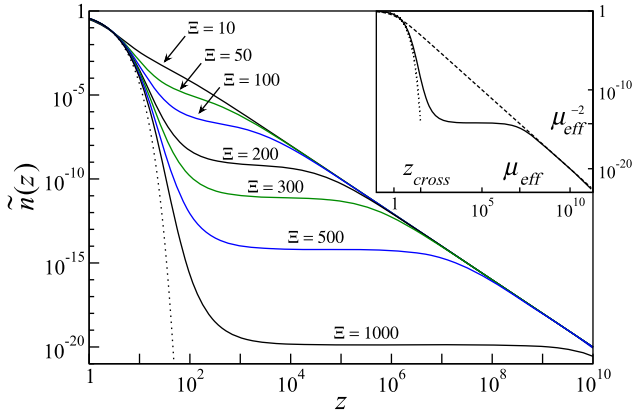

Figure 7. Scenario for the density large-distance asymptotics. The SC limiting behaviour on the left-hand side is displayed with the dotted line. The inset shows the crossover distance z_{cross} and the effective Gouy–Chapman length μ_{eff} for $\Xi = 500$.

trend. For $\Xi = 100$, the MC result clearly follows the exponential profile at $\tilde{z} < 10$ [18], then crosses over to a longer range decay, following a trend that is reminiscent of that observed within the correlation-hole approach (same shape in the log–log plot presented). Observing properly the PB algebraic tail in $1/z^2$, with MC at $\Xi > 100$, would require significantly larger systems, a relative accuracy on the profiles better than 10^{-6}, and is beyond our scope. For this reason and in order to study nevertheless the crossover to mean-field, we will in the remainder relinquish MC method and focus on the self-consistent treatment, which is considerable simpler to solve.

5.3. Discussion of asymptotic features

We wish to investigate the behaviour of ionic density at large distances, to first test the relevance of the correction worked out in Equation (49), but also to discuss the crossover to the mean-field regime. Figure 6 extracts the correction to the PB profile and compares it to the predicted functional form in $\Xi \log(1+z)/(1+z)^3$. This is achieved through the computation of the following quantity:

$$Q(z) = \frac{\widetilde{n}(z) - (1+z)^{-2}}{-2/3 \log(1+z)/(1+z)^3}. \tag{50}$$

It is observed that for $\Xi < 10$, Q saturates at large distance close to the expected value Ξ. For $\Xi = 50$ (and higher), the range of distances probed does not allow to reach large enough z to observe the phenomenon.

For $\Xi > 50$, the large-z density profile exhibits a new property, that is only beginning to emerge in Figure 5. This is illustrated in Figure 7: the expected exponential SC regime at short z and mean-field tail at large z are connected by a plateau, starting at the crossover length z_{cross}, where the density is quasi-constant. To be more specific, the existence of a plateau followed by a z^{-2} decay is precisely the PB prediction, with an effective Gouy–Chapman length μ_{eff}, and a density

$$\tilde{n}(z) = \frac{1}{(z+\mu_{\text{eff}})^2}. \tag{51}$$

Thus, for $z < \mu_{\text{eff}}$ (but $z > z_{\text{cross}}$), the density profile is flat, while for $z > \mu_{\text{eff}}$, it decays algebraically. Keeping in mind that by its definition in Equation (3), a Gouy–Chapman length scales like the inverse plate charge, it is natural to expect μ_{eff} to largely exceed the bare Gouy–Chapman length. Indeed, the PB-like profile sets in for $z > z_{\text{cross}}$ and subsumes all non-linear screening effects at work for $0 < z < z_{\text{cross}}$ into an effective plate surface charge, thus significantly smaller than σ. We recall that z, z_{cross} and μ_{eff} are dimensionless distances, measured in units of the actual Gouy-Chapman length (3).

It can be noted that the large-z expansion of Equation (51) yields $\tilde{n} \sim 1/z^2 - 2\mu_{\text{eff}}/z^3$. The resulting correction to the $1/z^2$ tail is of smaller order than the term in $\log z/z^3$ stemming from Equation (49). Hence, the value of μ_{eff} cannot be simply extracted from the asymptotic tail of the profile, but at smaller distances, where Equation (51) is relevant.[1] The plateau seen in Figure 7 illustrates this point: for $z > z_{\text{cross}}$, Equation (51) states that $\tilde{n}^{-1/2}$ increases linearly with distance, so that the quantity displayed in Figure 8 offers a convenient measure of the effective Gouy–Chapman length. It can be observed in Figure 8 that for $\Xi = 10$, one cannot properly extract a μ_{eff}, which is consistent with the data in Figure 5 (absence of a well-defined plateau). The inset of Figure 8, where the line shown has equation $y = x + 0.62$,

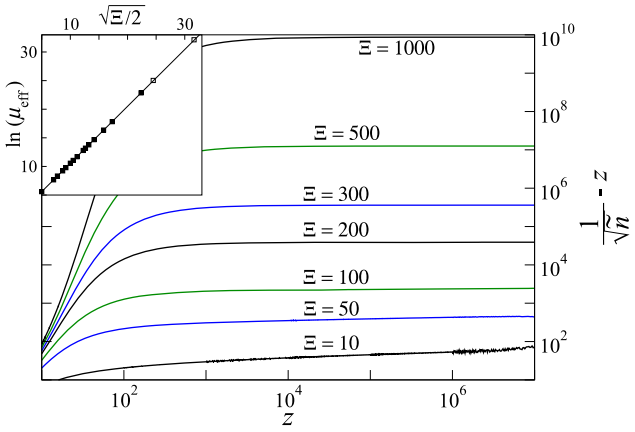

Figure 8. Extraction of the effective Gouy–Chapman length μ_{eff}, from the plot of $1/\sqrt{\tilde{n}} - z$, for Ξ between 10 and 1000. The plateau reached defines μ_{eff}. The inset shows how the resulting effective length depends on the coupling parameter. The line has slope 1.

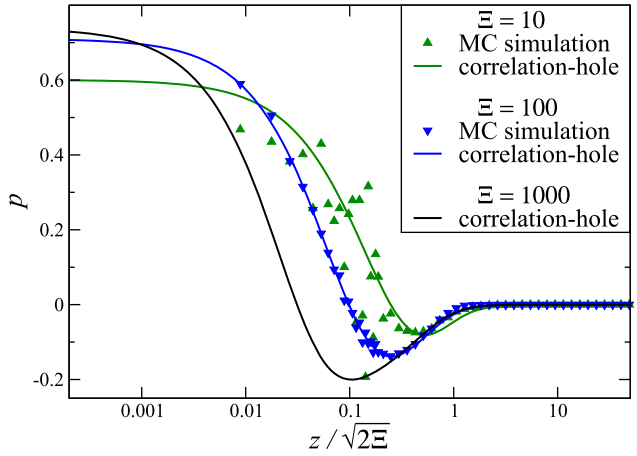

Figure 9. Implementing our mean-field probe. The vanishing of the local pressure $p(z)$, as defined in Equation (55), signals the PB regime. On the x-axis, distances have been rescaled by $z_{\text{cross}} = \sqrt{2\Xi}$. A system with $\Xi < 1$ exhibits a flat $p = 0$ curve, since mean-field holds at all distances. For large enough Ξ, p starts at 3/4 for small z (since $\tilde{n} = \exp(-z)$ locally holds), then reaches a minimum value close to $-1/4$, before vanishing on a scale z_{cross}. Symbols are for MC, and the curves for the correlation-hole theory.

then indicates that μ_{eff} changes with Ξ as

$$\log \mu_{\text{eff}} \sim \sqrt{\frac{\Xi}{2}} + \text{cst.} \tag{52}$$

This in turn sets the crossover distance to be

$$z_{\text{cross}} \sim \sqrt{2\,\Xi}, \tag{53}$$

by equating e^{-z} with $1/\mu_{\text{eff}}^2$ at z_{cross}. It does not come as a surprise to recover here the value of the correlation-hole size [20,22], see Equation (21) which reads $\tilde{R}^2 = 2\Xi$. The effective length μ_{eff} diverges with Ξ, such that $\log \mu_{\text{eff}}$ is linear in $\sqrt{\Xi}$, a conclusion also reached in [22]. Large values of μ_{eff} were observed numerically as well in the case of counter-ions around charged cylinders [65].

Finally, we present an operational way to decide when a system with an arbitrary Ξ is in the mean-field regime. The idea is to take advantage of the fact that the stress tensor is divergence-free [66]. For mean-field theories, this yields an extended contact theorem (not only at $z = 0$, but at any z). In the present planar geometry, this means that, using dimensionless quantities

$$p(z) \equiv \tilde{n}(z) - \tfrac{1}{4}[\phi'(z)]^2 = 0. \tag{54}$$

To check for that identity with numerically obtained results, one could compute the correct potential ϕ, from integrating the charge density. However, keeping in mind that we seek here a mean-field probe, it is more convenient to assume $\phi = \log \tilde{n}$ and we arrive at

$$p(z) \equiv \tilde{n}(z) - \tfrac{1}{4}[\partial_z \log \tilde{n}]^2 = 0. \tag{55}$$

Deviations of $p(z)$ from 0 provide a (sufficient) condition for mean-field violation. The fact that $p = 0$ within a mean-field treatment is a consequence of the contact theorem that reads $p(0) = 0$. It indicates that the pressure vanishes in our setting (single-plate problem, corresponding to a two-plate in interaction, in the limit where inter-plate distance is infinite). Figure 9 corroborates the existence of a PB tail, at large enough distances. Yet, a word of caution is in order here. It can rightfully be argued that a quantity such as $p(z)$ may only distinguish exponential profiles from algebraic ones, but that any density of the type $\tilde{n} \propto (\mu_{\text{eff}} + z)^{\alpha}$ yields $p \to 0$ for all $\alpha > 0$, and not only $\alpha = 2$. A possible solution would be to consider the ratio of the two terms subtracted in (55), rather than their difference; the ratio goes to a constant for the PB behaviour only ($\alpha = 2$). However, this has a drawback: it amplifies the contribution of any residual exponential tail in the density and requires larger distances to qualify the density as PB-like. A point to keep in mind though is that our probe (55) is more interesting for a two-plate system where the real (e.g. MC) pressure P is non-vanishing, rather than for the one-plate situation. Indeed, in such a case, comparing $p(z)$ to P can be viewed as signalling the mean-field regime.

6. Concluding remarks

We have studied a system of identical counter-ions near a wall carrying a uniform surface charge density, in thermal equilibrium. This is probably the simplest model of the electrical double layer, depending only on one parameter, the coupling constant Ξ. It provides an interesting

test-bench, since both Weak Coupling (WC) and Strong Coupling (SC) limits are known.

We have proposed a method which combines physical ideas from both WC and SC regimes. From the WC side, the particle density is determined by the Boltzmann factor of the mean potential. From the SC side, there is a cylindrical correlation hole around each particle, inaccessible to other particles, which modifies the value of the mean potential. The theory is simple by its construction and leads to a non-linear integral equation, similar to the PB one, which converges quickly in an iterative scheme.

Remarkably, all exact constraints are respected by our correlation-hole theory, for all coupling constants. The contact theorem for the particle density at the wall holds. The WC and SC limits are reproduced as well, and the correction to the SC limit $\Xi \to \infty$ is proportional to $1/\sqrt{\Xi}$, in accordance with recent approaches and MC simulations. For large distances from the wall and at arbitrary Ξ, the algebraic mean-field density profile is recovered. Moreover, we showed that the corresponding subleading correction, in $\Xi \log z/z^3$, is of the same form as found in a loop-wise field theoretic treatment of fluctuations beyond Poisson–Boltzmann [16]. Focusing on the approach to mean-field behaviour at large distances, we showed that beyond a crossover distance $z_{\rm cross}$ (coinciding with the hole size), the density takes a Poisson–Boltzmann form. This allows to define an effective Gouy–Chapman length to describe the density tail. In units of the bare length μ, it behaves as $\mu_{\rm eff} \propto \exp(\sqrt{\Xi/2})$ and quickly grows with Ξ. This is a signature of efficient non-linear screening, leading to a small effective surface charge for the plate, as far as its large-scale potential is concerned. Introducing a 'mean-field probe', $p(z)$ in Equation (55), we recover the results of a direct analysis of the numerical profiles.

For the sake of completeness, we also considered the situation of two parallel uniformly charged plates (surface charge density σe), at distance d, sandwiching a slab of counter-ions. There, an ambiguity arises when enforcing the idea of a correlation hole. Indeed, we have to distinguish between the two limits $d \to \infty$ and $d \to 0$. Accepting the cylinder form of the correlation hole, the cylinder radius is given by formula (21) if $d \to \infty$, i.e. $\sigma\pi R_\infty^2 = q$, and by $2\sigma\pi R_0^2 = q$ if $d \to 0$. A possible, d-dependent interpolation formula for the correlation-hole size might be relevant, but for simplicity, we took the same prescription as in the one-plate case, Equation (21). The alternative choice turned out to be slightly worse. The equation of state of this system, as measured in MC simulations, is reported in Figure 10. To test our correlation-hole approach (accurate at both small and large couplings), we concentrate in Figure 10 on

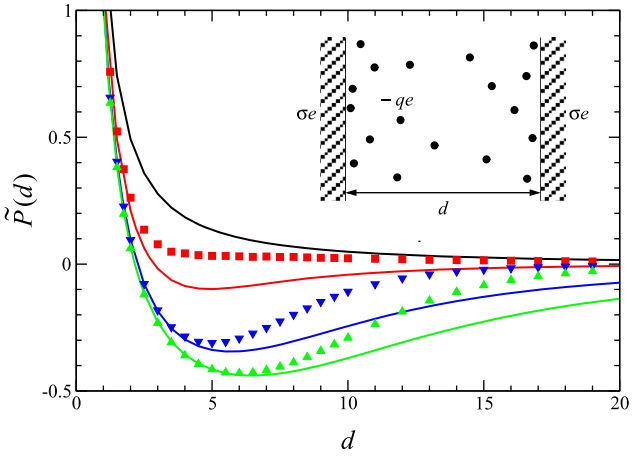

Figure 10. Interplate pressure versus rescaled distance, for $\Xi = 1$, 10, 50 and 100 (from top to bottom). MC results (symbols) are compared to the prediction of the correlation-hole theory (lines). The rescaled pressure is defined as $\tilde{P} = P/(k_{\rm B}T2\pi\ell_{\rm B}\sigma^2)$ and is measured from the contact theorem.

intermediate coupling strengths, where the phenomenon of like-charge attraction sets in [3,17,19,56]. We see that the qualitative features of the pressure are well captured, with an agreement that is quantitative for small distances, up to the range where like-charge attraction is maximal (minimum of the pressure). The asymptotic decay to vanishing pressure then takes place over too large distances, as compared to MC. The correlation-hole idea there overestimates the SC non-mean-field features; correcting for this deficiency is left for future work. Yet, it is noteworthy that the present theory captures here also a number of exact features. Not only is the proper equation of state recovered when $\Xi \to 0$ and $\Xi \to \infty$, but also the pressure minimum arises at $z \propto \Xi^{1/4}$, as found in MC simulations [21,50].

Note

1. Yet, as alluded to above, reaching the z-range where the log correction is relevant becomes in practice impossible when increasing Ξ. For instance, we would need $z > 10^6$ for $\Xi = 50$ and already $z > 10^{29}$ for $\Xi = 100$. Thus, the log correction can only be probed at $\Xi < 50$.

Disclosure statement

No potential conflict of interest was reported by the authors.

Funding

It is a pleasure to dedicate this work to Daan Frenkel as a tribute to his exceptional human and scientific qualities (depth, vista, swiftness), be it as a mentor or a colleague. To counter-quote Churchill, Daan is a modest man, who does not have much to be modest about. The support received from VEGA Grant No. 2/0003/18 is acknowledged. The work was funded

by the European Union's Horizon 2020 research and innovation programme under ETN grant 674979-NANOTRANS. M.T. acknowledges financial support by the Swedish Research Council (621-2014-4387).

References

[1] Ph. Attard, Adv. Chem. Phys. **92**, 1 (1996).
[2] J.P. Hansen and H. Löwen, Annu. Rev. Phys. Chem. **51**, 209 (2000).
[3] R. Messina, J. Phys. Condens. Matter. **21**, 113102 (2009).
[4] A. Khan, B. Jönsson and H. Wennerström, J. Chem. Phys. **89**, 5180 (1985).
[5] R. Kjellander, S. Marčelja and J.P. Quirk, J. Colloid Interface Sci. **126**, 194 (1988).
[6] V.A. Bloomfield, Biopolymers **31**, 1471 (1991).
[7] D.C. Rau and V.A. Pargesian, Biophys. J. **61**, 246 (1992);ibid. 61, 260 (1992).
[8] P. Kékicheff, S. Marčelja, T.J. Senden and V.E. Shubin, J. Chem. Phys. **99**, 6098 (1993).
[9] M. Dubois, T. Zemb, N. Fuller, R.P. Rand and V.A. Pargesian, J. Chem. Phys. **108**, 7855 (1998).
[10] L. Gulbrand, B. Jönsson, H. Wennerström and P. Linse, J. Chem. Phys. **80**, 2221 (1984).
[11] R. Kjellander and S. Marčelja, Chem. Phys. Lett. **112**, 49 (1984).
[12] D. Bratko, B. Jönsson and H. Wennerström, Chem. Phys. Lett. **128**, 449 (1986).
[13] N. Grønbech-Jensen, R.J. Mashl, R.F. Bruinsma and W.M. Gelbart, Phys. Rev. Lett. **78**, 2477 (1997).
[14] L. Belloni, J. Phys. Condens. Matter. **12**, R549 (2000).
[15] C. Holm, P. Kékicheff and R. Podgornik, Electrostatic Effects in Soft Matter and Biophysics, Proceedings of the NATO Advanced Research Workshop on Electrostatic Effects in Soft Matter and Biophysics, Les Houches (Springer, 2000).
[16] R.R. Netz and H. Orland, Eur. Phys. J. E **1**, 203 (2000).
[17] A.G. Moreira and R.R. Netz, Europhys. Lett. **52**, 705 (2000);Phys. Rev. Lett. **87**, 078301 (2001).
[18] R.R. Netz, Eur. Phys. J. E **5**, 557 (2001);A.G. Moreira and R.R. Netz, Eur. Phys. J. E **8**, 33 (2002).
[19] Y. Levin, Rep. Prog. Phys. **65**, 1577 (2002).
[20] Y. Burak, D. Andelman and H. Orland, Phys. Rev. E **70**, 016102 (2004).
[21] Y.G. Chen and J.D. Weeks, Proc. Natl. Acad. Sci. U.S.A. **103**, 7560 (2006).J.M. Rodgers, C. Kaur and Y.G. Chen, Phys. Rev. Lett. **97**, 097801 (2006).
[22] C.D. Santangelo, Phys. Rev. E **73**, 041512 (2006).
[23] T.-Y. Wang, H.-T. Li, Y.-J. Sheng and H.-K. Tsao, J. Chem. Phys. **129**, 204504 (2008).
[24] A.R. Denton, J. Phys. Condens. Matter. **20**, 494230 (2008).
[25] M.M. Hatlo and L. Lue, Europhys. Lett. **89**, 25002 (2010).
[26] G. Téllez and E. Trizac, Phys. Rev. E **92**, 042134 (2015).
[27] J.-S. Sin, H.-C. Pak, K.-I. Kim, K.-C. Ri, D.-Y. Ju, N.-H. Kima and C.-S. Sina, Phys. Chem. Chem. Phys. **18**, 234 (2016).
[28] L. Šamaj, A.P. dos Santos, Y. Levin and E. Trizac, Soft Matter **12**, 8768 (2016).
[29] E. Raspaud, M. da Conceiçao and F. Livolant, Phys. Rev. Lett. **84**, 2533 (2000).
[30] T. Palberg, M. Medebach, N. Garbow, M. Evers, A.B. Fontecha, H. Reiber and E. Bartsch, J. Phys. Condens. Matter **16**, S4039 (2004).
[31] M. Brunner, J. Dobnikar, H.-H. von Grünberg and C. Bechinger, Phys. Rev. Lett. **92**, 078301 (2004).
[32] C. Haro-Pérez, M. Quesada-Pérez, J. Callejas-Fernández, P. Schurtenberger and R. Hidalgo-Alvarez, J. Phys. Condens. Matter **18**, L363 (2006).
[33] L.-F. Rojas-Ochoa, R. Castañeda-Priego, V. Lobaskin, A. Stradner, F. Scheffold and P. Schurtenberger, Phys. Rev. Lett. **100**, 178304 (2008).
[34] Ph.A. Martin, Rev. Mod. Phys. **60**, 1075 (1988).
[35] L. Šamaj, Eur. Phys. J. E **36**, 100 (2013).
[36] D. Andelman, in *Soft Condensed Matter Physics in Molecular and Cell Biology*, edited by W.C.K. Poon and D.Andelman (Taylor & Francis, New York, 2006).
[37] P. Attard, D.J. Mitchell and B.W. Ninham, J. Chem. Phys. **88**, 4987 (1988).
[38] R. Podgornik, J. Phys. A **23**, 275 (1990).
[39] B.I. Shklovskii, Phys. Rev. E **60**, 5802 (1999).
[40] M.C. Barbosa, M. Deserno and C. Holm, Europhys. Lett. **52**, 80 (2000).
[41] R. Golestanian, Europhys. Lett. **52**, 47 (2000).
[42] A. Naji, S. Jungblut, A.G. Moreira and R.R. Netz, Physica A **352**, 131 (2005).
[43] A. Naji and R.R. Netz, Phys. Rev. Lett. **95**, 185703 (2005); Phys. Rev. E **73**, 056105 (2006).
[44] M. Kanduč and R. Podgornik, Eur. Phys. J. E **23**, 265 (2007).
[45] M. Kanduč, M. Trulsson, A. Naji, Y. Burak, J. Forsman and R. Podgornik, Phys. Rev. E **78**, 061105 (2008).
[46] Y.S. Jho, M. Kanduč, A. Naji, R. Podgornik, M.W. Kim and P.A. Pincus, Phys. Rev. Lett. **101**, 188101 (2008).
[47] D.S. Dean, R.R. Horgan, A. Naji and R. Podgornik, J. Chem. Phys. **130**, 094504 (2009).
[48] M. Kanduč, A. Naji, J. Forsman and R. Podgornik, J. Chem. Phys. **132**, 124701 (2010).
[49] V.I. Perel and B.I. Shklovskii, Physica A **274**, 446 (1999);B. I. Shklovskii, Phys. Rev. E **60**, 5802 (1999).
[50] L. Šamaj and E. Trizac, Phys. Rev. Lett. **106**, 078301 (2011);Phys. Rev. E **84**, 041401 (2011).
[51] M.M. Hatlo and L. Lue, Soft Matter **5**, 125 (2009).
[52] S. Nordholm, Chem. Phys. Lett. **105**, 302 (1984).
[53] I. Rouzina and V.A. Bloomfield, J. Phys. Chem. **100**, 9977 (1996).
[54] J. Forsman, J. Phys. Chem. B **108**, 9236 (2004).
[55] A. Bakhshandeh, A.P. dos Santos and Y. Levin, Phys. Rev. Lett. **107**, 107801 (2011).
[56] E. Trizac and L. Šamaj, in *Proceedings of the International School of Physics Enrico Fermi*, edited by C. Bechinger, F. Sciortino and P. Ziherl, Vol. 184 (IOS, Amsterdam, 2013), p. 61.
[57] D. Henderson and L. Blum, J. Chem. Phys. **69**, 5441 (1978);D. Henderson, L. Blum and J.L. Lebowitz, J. Electroanal. Chem. (102), 315 (1979).
[58] S.L. Carnie and D.Y.C. Chan, J. Chem. Phys. **74**, 1293 (1981).
[59] H. Wennerström, B. Jönsson and P. Linse, J. Chem. Phys. **76**, 4665 (1982).
[60] A.P. dos Santos, A. Diehl and Y. Levin, J. Chem. Phys. **130**, 124110 (2009).

[61] J.-P. Mallarino, G. Téllez and E. Trizac, Mol. Phys. **113**, 2409 (2015).
[62] I.-C. Yeh and M.L. Berkowitz, J. Chem. Phys. **111**, 3155 (1999).
[63] M. Mazars, J.-M. Caillol, J.-J. Weis and D. Levesque, Condens. Matter Phys. **4**, 697 (2001).
[64] M. Trulsson, E. Trizac and L. Šamaj, J. Phys. Condens. Matter **30**, 035001 (2018).
[65] J.-P. Mallarino, G. Téllez and E. Trizac, J. Phys. Chem. B **117**, 12702 (2013).
[66] E. Trizac, Langmuir **17**, 4793 (2001).

Appendix. MC simulations

MC Metropolis simulations were carried out by using 256 point charges located between two hard and planar surfaces, one of them having a surface charge density of $e\sigma$ and the other being uncharged, in a quasi-2D slab geometry at different separations. The simulation cells were periodic in all directions with an extra vacuum slab in the z-direction inaccessible to the point charges. This set-up allowed us to use standard Ewald simulation techniques with only minor corrections for the imposed quasi-2D geometry [62,63]. The vacuum slab was chosen large enough such that it did not influence the results (i.e. the periodic images in the z-direction were too far from each other to influence each other), typically larger than a couple of thousands of Gouy–Chapman lengths. The separation between the surfaces was fixed to $4 \cdot 10^3$ Gouy–Chapman lengths, practically yielding a zero particle density at the uncharged wall. Standard trial displacement moves were performed with an acceptance ratio of around 30% over 10^5 MC cycles, where one MC cycle involved 256 trial displacements. MC simulations were also performed for two parallel uniformly charged plates using the same techniques as described above (with the exception of now having both surfaces charged). For this purpose, we doubled the number of point charges. Pressures were collected using the contact theorem by an interpolation of the densities close to the surfaces and were sampled for various interplate separations. Consistency checks were also performed by evaluating the pressure over the mid-plane, which yielded the exact same pressures.